ASCA observations of type-2 Seyfert Galaxies: II The Importance of X-ray Scattering and Reflection

T.J.Turner [1,2], I.M. George [1,2], K. Nandra [1,3], R.F. Mushotzky[1],

ABSTRACT

We discuss the importance of X-ray scattering and Compton reflection in type-2 Seyfert Galaxies, based upon the analysis of *ASCA* observations of 25 such sources. Consideration of the iron Kα, [OIII] line and X-ray variability suggest that NGC 1068, NGC 4945, NGC 2992, Mrk 3, Mrk 463E and Mrk 273 are dominated by reprocessed X-rays. We examine the properties of these sources in more detail.

We find that the iron Kα complex contains significant contributions from neutral and high-ionization species of iron. Compton reflection, hot gas and starburst emission all appear to make significant contributions to the observed X-ray spectra.

Mrk 3 is the only source in this subsample which does not have a significant starburst contamination. The *ASCA* spectrum below 3 keV is dominated by hot scattering gas with $U_X \sim 5$, $N_H \sim 4 \times 10^{23}\mathrm{cm}^{-2}$. This material is more highly ionized than the zone of material comprising the warm absorber seen in Seyfert 1 galaxies, but may contain a contribution from shock-heated gas associated with the jet. Estimates of the X-ray scattering fraction cover 0.25 – 5%. The spectrum above 3 keV appears to be dominated by a Compton reflection component although there is evidence that the primary continuum component becomes visible close to ~ 10 keV.

Subject headings: galaxies: active — galaxies: nuclei — line: formation — X-rays: galaxies

[1]Laboratory for High Energy Astrophysics, Code 660, NASA/Goddard Space Flight Center, Greenbelt, MD 20771

[2]Universities Space Research Association

[3]NAS/NRC Research Associate

1. Introduction

The optical spectra of most nearby active galactic nuclei (AGN) are dominated by narrow optical lines (e.g. Lawrence 1991) and are therefore broadly classified as type-2 Seyfert galaxies. However, broad optical lines with characteristics similar to those observed in Seyfert 1 galaxies were discovered in the polarized light from NGC 1068 (Antonucci & Miller 1985). It was suggested that the polarization arose as a result of electron scattering, implying that the optical broad-line-region in NGC 1068 is only visible in scattered light. When several more examples of the phenomenon were found (Miller & Goodrich 1990) a general model emerged in which the nuclear spectra of both Seyfert types 1 and 2 are the same, but the nuclear regions of type 1 are observed directly while Seyfert 2 nuclei are hidden behind a large column of obscuring material. The simplest geometry for the obscuring material is a torus. This allows orientation-dependant obscuration, and hence can explain the existence of the type-1 and type-2 Seyfert galaxies. Hubble Space Telescope (*HST*) observations have now resolved a torus in the AGN NGC 4261 (Ferrarese, Ford & Jaffe 1996). Such a torus allows the existence of some lines-of-sight for which radiation from within the torus can only be viewed via scattering. The high opacity of the obscuring material makes it difficult to directly observe the central engines of Seyfert 2 galaxies at most wavelengths. Medium energy X-rays can penetrate column densities of up to $\sim 10^{24}$ cm^{-2}, allowing a direct view of some type-2 nuclei, but observations of sources with even larger columns should reveal predominantly scattered or reflected X-rays below 10 keV.

In a companion paper (Turner et al. 1997, hereafter Paper I) we presented the data analysis results of *ASCA* observations of a sample of 17 Seyfert 2 galaxies, plus 8 Narrow Emission Line Galaxies (NELGs). Paper I dealt with temporal and spectral X-ray results from those two classes of AGN together. The observations were drawn from the public archive, and the sources do not comprise a complete sample. The data selection, reduction and analysis are described in detail in Nandra et al. 1997 (hereafter N97) and Paper I. The sources in which we observe the nucleus through the absorber will be discussed in another paper (Turner et al. 1997b). In the present paper we determine which sources from the original sample are most likely to be dominated by reprocessed X-ray emission, and then examine the properties of this subset in detail.

2. Signatures of Reprocessed X-ray Emission

Iron Kα lines in AGN arise via reprocessing of the primary X-rays. If Kα lines of very high equivalent width are observed, this is an indication that one is viewing a spectrum

dominated by reprocessing. For Seyfert 2 galaxies, it is appropriate to consider two types of reprocessing, which we shall refer to as "Compton reflection" and "scattering". We use the term Compton reflection (or simply "reflection") to mean reprocessing of X-rays via Compton scattering and fluorescence by material which is optically thick to electron scattering. We use the term "scattering" to apply to the case where the optical depth to electron scattering is $0 < \tau < 1$.

In Seyfert 1 galaxies, the iron Kα lines are thought to arise via Compton reflection from an accretion disk (e.g., N97), which produces lines of equivalent width $\sim$ few hundred eV with respect to the directly observed continuum (e.g. George & Fabian 1991). However, the equivalent width of the iron Kα line can be as high as a few keV with respect to the Compton-reflected continuum (George & Fabian 1991; Matt et al. 1991). Such a situation is somewhat unlikely in the case of an accretion disk, as the central continuum and iron line are both produced in a very small region and obscuring one without the other would require an unusual geometry. However, the reflection may also occur at the inner surface of the obscuring material, possibly the torus, and the orientation and opening angle can then allow a view of the inner surface, but not the illuminating source. Some early *ASCA* results showed that Compton reflection of nuclear radiation from optically thick material can be an important component of Seyfert 2 galaxies. The Circinus galaxy (Matt et al. 1996) and NGC 6552 (Fukazawa et al. 1994) show strong reflection components dominating the spectra even below 10 keV.

If the iron Kα line is produced in optically thin gas then its observed equivalent width can also be large as long as the direct continuum is not observed. The line equivalent width is a strong function of the ionization-state of the material (which is also the case for the reflected iron lines, but both the disk and torus are thought to be relatively neutral). For low ionization-states the equivalent width of the iron K-shell line, measured against the scattered nuclear emission (plus free-free and bound-free emission from the scattering gas) can be as high as ~ 1 keV for the 6.4 keV line (Netzer 1996), and could appear to be up to a few keV for an iron line blend.

Although it is tempting to interpret lines of high equivalent width as evidence for a dominant reflected or scattered component, high equivalent widths can also arise if the ionizing radiation is anisotropic (e.g. Ghisellini et al. 1991) or if there is a significant lag between a fall in the continuum flux and the reprocessed spectrum. Indeed, Weaver et al. (1996) suggested a 16 year lag between a drop in continuum and line fluxes, to explain the large equivalent width in the iron Kα line for NGC 2992 at the *ASCA* epoch. Thus, when assessing whether or not a source is dominated by reprocessing, it is important to take other evidence into account.

An alternative method of determining whether a type-2 Seyfert galaxy contains a hidden X-ray source is by examining the flux in the [OIII] λ5007 emission line (hereafter simply referred to as [OIII]) observed in the optical regime. Mulchaey et al. (1994) found a strong correlation between [OIII] and hard X-ray flux in a sample of Seyfert 1 galaxies. This provides an independant estimate of the nuclear X-ray luminosity for Seyfert 2 galaxies for comparison with the observed X-ray luminosity. If the observed X-ray luminosity is substantially less than that predicted by [OIII] this is an indication that the X-ray emission is being observed indirectly, with only a fraction of the total luminosity reaching our line-of-sight.

3. Identification of the reflected/scattered sources

A summary of the *ASCA* sample is detailed in Table 1. We now consider the properties of these sources in relation to the above discussion, to determine which Seyfert 2 galaxies are likely to be dominated by reprocessed emission.

3.1. Iron line equivalent width

In Paper I we found the 6-7 keV regime of low redshift type-2 Seyfert galaxies to be dominated by emission at 6.4 keV. This indicates that a large fraction of the iron Kα line flux is produced in gas with ionization-state $<$ Fe XVI. Furthermore, such a line is not generally observed in starburst galaxies (Ptak et al. 1997), and certainly not with such a high equivalent-width, indicating that these lines are related to the active nucleus. We found such a line in 72% of the sample sources at $>$ 99% confidence. Fig. 1 (adapted from a figure in Paper I) shows the equivalent widths of the 6.4 keV lines versus X-ray absorbing column (except in the case of NGC 6251, where the 6.68 keV line is the only iron Kα line detected, and so this is plotted). All detected sources are shown from Paper I, except NGC 1667 which had a best-fit line equivalent width of zero, and an upper limit of 3 keV. The line equivalent widths are measured against the hard X-ray continuum component (i.e. the component dominating the fit over 6 - 8 keV, from the best-fit continuum model, see Paper I for details). First we consider two plausible processes which could produce the line emission *without* invoking a dominant reflected or scattered component.

Line emission could be produced by transmission through the line-of-sight absorber. The dot-dash line in Fig 1 denotes the equivalent width of iron Kα predicted to be produced by a uniform shell of neutral material with solar abundances subtending 4π to a continuum

source of photon index $\Gamma = 2.0$ (Leahy & Creighton 1993). It is immediately obvious that a substantial fraction of the emission lines in our sample cannot be produced by such a process. Non-uniformity of the absorbing material cannot explain these discrepancies. If we view the source with a line-of-sight through absorption lower than the mean column, then we see more continuum photons at 6.4 keV, reducing the apparent equivalent width of the iron Kα line. In the opposite case, enhancements in the line equivalent width can be produced, but large equivalent widths ($\gtrsim 100$ eV) are only produced when the line-of-sight column is very high $\gg 10^{23}$ cm^{-2}. This is not the case for the sources which are discrepant with the Leahy & Creighton line.

The mean equivalent width of the emission lines in Seyfert 1 galaxies is 230 ± 60 eV (N97), and most of this is thought to be attributable to Compton reflection of nuclear X-rays from the surface of the putative accretion disk. Further enhancement of this value in Seyfert 2 galaxies could be afforded if the direct continuum is suppressed by absorption, but the Compton-reflection component is not. As we have noted above, if the Compton reflection arises in an accretion disk, this is not very likely. It is, however, plausible if the absorbing material (possibly, but not necessarily the torus) is responsible for the Compton reflection. The dashed line (Fig. 1) shows the predicted equivalent width from reflection as a function of $N_{\rm H}$, assuming that only the power-law is absorbed, but that the reflection component remains unchanged. Many of our sources lie significantly above this line also, which in any case only implies large (~ 1 keV) equivalent widths for very high columns ($\gg 10^{24}$ cm^{-2}). The direct continuum in the 2-10 keV band is then so heavily suppressed that the sources are dominated by the reflection component anyway.

In cases where a source lies significantly above both of these two model lines, we consider there to be good evidence that the *ASCA* spectrum is dominated by reprocessed emission. These are NGC 1068; Mrk 3; NGC 2992 and NGC 4945. A number of other sources (Mrk 463E; NGC 6251; NGC 4968; NGC 5135 and Mrk 273) have best-fit equivalent widths higher than the model lines, but are formally consistent with one or both. These sources are could plausibly be dominated by reprocessing, but such a conclusion is not warranted based on the Kα line strengths alone and require supporting evidence. We now consider such evidence.

3.2. [OIII] measurements

Table 1 shows the 2-10 keV absorption-corrected luminosity [4] predicted based upon [OIII] line flux measurements (see Mulchaey et al. 1994, Polletta et al. 1996 and references therein), and the measured (absorption-corrected) 2-10 keV luminosity for each source. Mulchaey et al. (1994) find the relationship between hard X-ray flux and [OIII] flux is consistent with being the same for the Seyfert 1 and Seyfert 2 galaxies in their sample. There is a larger scatter in the distribution in the case of the Seyfert 2 sample, as might be expected because that sample contains some sources for which the hard X-ray flux is just the scattered X-rays. For that reason, we use the more tightly-determined correlation for the Seyfert 1 galaxies as the basis of our calculation. The resulting intrinsic luminosities are tabulated and plotted against the observed values (from Paper I, Table 12) in Fig. 2.

Unfortunately the [OIII] flux can include some unresolved contribution from starburst emission, depending on the aperture used and the level and location of starburst activity in the host. We might expect some predicted luminosities to be too high because of this confusion. We also expect scatter in the plot due to variability and the imperfect nature of the correlation between [OIII] and hard X-ray luminosity. Given these uncertainties we highlight (by naming the sources on the plot) only those sources whose predicted luminosities exceed the observed by a factor > 15. This confirms the suggestion of a hidden X-ray continuum in NGC 1068, Mrk 3 and NGC 2992, which we had already concluded based on the iron line evidence. The lack of an [OIII] flux measurement for NGC 4945 excludes that source from this test. However, heavy obscuration in NGC 4945 is well established. Done et al. (1996) used the combined *Ginga*, *ASCA* and *OSSE* data to confirm the Iwasawa (1994) result that the nucleus of NGC 4945 is so heavily absorbed that the direct component is only visible above 10 keV.

Examination of the [OIII] flux also indicates a hidden X-ray continuum in Mrk 273, Mrk 463E, NGC 4507, NGC 1667 and NGC 5695. The cases for reprocessing in Mrk 273 and Mrk 463E now become much stronger, as the iron Kα lines also had a very high equivalent width (although the constraints were such that an alternative origin could not be ruled out). The iron Kα equivalent widths indicate consistency with an origin in the line-of-sight absorber in NGC 4507 and NGC 1667 (although the latter in particular is highly uncertain). Thus we conclude that the evidence for extensive reprocessing in these cases is inconclusive and we do not consider NGC 4507 and NGC 1667 in detail in this paper. NGC 5695 has no observed *ASCA* flux (just an upper limit) and so it is not plotted in Fig. 2. However, if the intrinsic luminosity implied by the [OIII] flux was observed

[4] $H_0 = 50$ km s^{-1}Mpc^{-1} and $q_0 = 0.5$ assumed throughout

directly, NGC 5695 would have been detected easily by *ASCA*. This suggests that the absorbing column exceeds a few 10^{24}cm^{-2}. Elongated narrow-line regions in some Seyfert galaxies appear to be ionized by a more intense radiation field than is directly observable, (e.g. Haniff, Wilson & Ward 1988, Pogge 1988, Tadhunter and Tsvetanov 1989). This provides supporting evidence for hidden nuclei in sources such as Mrk 3.

Finally, we note that NGC 6251 and NGC 4968, which showed (albeit poorly-constrained) iron Kα lines with high equivalent width do not show evidence for a hidden continuum based on the [OIII] measurements, and so we do not consider them further in this paper.

3.3. X-ray variability

Of the sources most likely to be dominated by reprocessed emission, only NGC 1068 was bright enough for us to search for rapid X-ray variability (Paper I). It did not vary significantly when sampled on a 128 s timescale. While several of the sources appear to show hard X-ray variability on timescales of years (Polletta et al. 1996), all cases except Mrk 3 are based upon comparison between *HEAO/A1* and *ASCA* or *Ginga*. The low angular resolution of *HEAO/A1* yields systematically high fluxes assigned to those measurements of many source fluxes in the Polletta et al. (1996) catalog. Thus we do not consider apparent flux variations which depend on the *HEAO/A1* measurements, to be reliable.

NGC 2992 is unique amongst the reprocessing-dominated sources because it shows correlated variability in the hard and soft X-ray regimes down to timescales of a few days (Weaver et al. 1996, Turner & Pounds 1989). This indicates that we are seeing the 0.5 - 10 keV flux directly. Thus Weaver et al. (1996) suggest that NGC 2992 has a strong observed iron Kα line because of a lag between direct and reprocessed flux, rather than due to obscuration of the nucleus. However, the 6.4 keV line is still inferred to arise by Compton reflection, and so we continue to include it in our consideration of the reprocessed source spectra.

Thus, taking the iron Kα, [OIII] line and variability evidence together, we are most confident that the *ASCA* observations are dominated by reprocessed X-rays in the cases of NGC 1068, NGC 4945, NGC 2992, Mrk 3, Mrk 463E and Mrk 273. For ease of reference we now denote these as "group C" sources and these are marked with squares on Fig. 1. For later reference we denote the sources lying on the Leahy and Creighton line to be "group A", and those with iron Kα equivalent widths lying between that line and 230 eV to be "group B". Group B sources have iron Kα lines consistent with those observed from

the relativistic accretion disk in Seyfert 1 galaxies (N97). The properties of group A and B sources will be discussed in a later paper (Turner et al. 1997b). We continue here by investigating what the X-ray properties of group C sources can tell us about conditions in the reprocessing media.

4. The nature of the reprocessing regions

4.1. Constraints from absorption

The absorbing columns detected in the reprocessed sources ($\sim 10^{22}\mathrm{cm}^{-2}$) do not necessarily represent the line-of-sight attenuation to the nucleus. Rather, they may represent opacity in the scattering gas. In principle, then, measurements of that absorption could be used to indicate the column density and ionization state of that medium. However, misleading spectral fit parameters can be obtained when fitting simple continuum models (Paper I) to spectra dominated by photoionized emission. To illustrate this point, Fig. 3 shows a typical emission spectrum from ionized absorbing gas observed in the line-of-sight to $\gtrsim 60\%$ of Seyfert 1 galaxies (Reynolds 1997; George et al. 1997). The gas has an ionization parameter $U_X \sim 0.125$ and column $N_H \sim 4 \times 10^{22}\mathrm{cm}^{-2}$, based on the analysis of *ASCA* observations of Seyfert 1 galaxies (see George et al. 1997 for details and the definition of U_X). For a demonstration we simulated a 40 ksec *ASCA* observation of the emission spectrum of the warm absorber gas and then fit the simulated spectrum with a model composed of an absorbed power-law plus a Raymond-Smith equilibrium plasma. We find a best-fitting spectrum with a flat power-law of $\Gamma = 0.87$ absorbed by a column $N_H = 1.8 \times 10^{22}\mathrm{cm}^{-2}$ plus an unabsorbed plasma with $kT = 0.86$ keV, with a fit-statistic of $\chi^2 = 424/331$. Both the fit parameters and acceptability are reminiscent of values obtained when fitting some Seyfert 2 galaxies with simple models (e.g. Paper I). Apparently, the presence of the emission spectrum from the scattering gas can mimic an absorbed flat power-law plus a soft thermal component.

If the warm absorber commonly seen in Seyfert 1 galaxies is the same material which scatters nuclear X-rays into our line of sight in the Seyfert 2 case, then we should expect the same distribution of ionization parameter and column for these components, and we discuss this in §6, in the context of the spectral results from Mrk 3. Krolik & Kriss (1995) suggest that an X-ray heated wind can produce both the warm absorber in Seyfert 1 galaxies, and warm scattering gas affording a view of the central nuclei of Seyfert 2 galaxies. The wind idea is supported by the blueshifts observed in the UV absorption systems in some QSOs and Seyfert galaxies. Those systems generally show blueshifts indicative of outflow velocities of a few hundred km/s. Observations to date of the X-ray absorber have been

insensitive to such small velocity shifts (George et al. 1997). In any case, velocity shifts might be most difficult to observe in type-2 Seyferts because the wind velocity vector could be almost perpendicular to our line-of-sight.

4.2. Constraints from emission

The strength of the iron Kα lines in the group C sources is a strong indication that they arise via reprocessing. As stated above, the majority of the line emission occurs close to 6.4 keV, suggesting an origin via reflection from the absorbing material. This component of the line profile is expected to be free of the relativistic effects evident in the iron Kα line profiles of Seyfert 1 galaxies (N97). Fig. 4 shows the individual ratios in the iron Kα regime, from reprocessed sources with the most significant iron lines, i.e. NGC 1068, Mrk 3, NGC 2992 and NGC 4945. Ratios are shown for the summed SIS plus GIS data, and the SIS data alone. The SIS data alone have superior energy resolution, but unfortunately our systematic method of analysis has left few significant SIS data bins at high energies. We note that Iwasawa et al. (1996) obtained a clearer SIS line profile for NGC 1068 by optimizing the data screening for that observation (the conservative criteria used in N97 and Paper I yield a low SIS exposure compared to the on-time of the observation in this case).

The SIS data can provide some useful information when the data/model ratios are co-added. The energy-scale of each SIS spectrum was redshift-corrected to the rest-frame of the source and then the average SIS instrument ratio was calculated utilizing all of the group C sources (versus the best continuum model in each case, from Paper I). Fig. 5 shows the result of this summation. The average SIS data/model ratio is shown, and the dotted Gaussian profile represents the SIS instrument response for a narrow line observed at a rest-energy of 6.4 keV. This plot does not show the actual line profile, rather the counts ratio compared to the best continuum model (to get the true profile you have to multiply the ratio plot by the continuum form). Excess flux is evident blueward and redward of 6.4 keV. The former seems most likely to indicate the presence of high-ionization species of iron Kα, which are present in NGC 1068, Mrk 3, NGC 4945, and NGC 2992 when tested on an individual basis (Paper I). Mrk 463E and Mrk 273 did not have sufficient signal-to-noise to detect features of a similar relative strength. All of the sources showed a significantly broad line when the iron Kα regime was modelled with a single gaussian, so the sources either have multiple unresolved components, like NGC 1068 (Marshall et al. 1993), or the iron Kα lines are broadened.

It therefore seems most likely that the spectra contain contributions both from

Compton reflection and the scattering gas, although as noted above, if the latter has multiple ionization states and the dominant one is relatively cool, this could account for a strong 6.4 keV component without the need for reflection. Of particular interest in this regard is the observation of a red wing to the line. This signature – which amounts to $\sim$ 10 per cent of the core flux – is not expected to be produced by scattering from an optically thin medium. The same feature is observed with the same equivalent width in the iron Kα profile of Seyfert 1 galaxies (N97). Iwasawa et al. (1996) noted the presence of a red-wing in the iron Kα line profile of NGC 1068. Those authors noted that it was consistent with the "Compton shoulder" expected from downscattering of 6.4 keV photons in a reflecting medium. The Mrk 3 and NGC 4945 profiles appear to show the same effect but NGC 2992 does not (Fig. 4, although the data do not allow us to place interesting constraints in this respect, Mrk 463E and Mrk 273 are inconclusive due to a lack of signal-to-noise in the 5-7 keV regime.) Iwasawa et al. (1996) state that the red wing in NGC 1068 is more likely to be attributed to a Compton shoulder than to the relativistic effects observed in Seyfert 1 galaxies, as the contribution of the relativistic disk should be observed only in scattered light. However, if the continuum is also scattered, the relativistic disk component would have the same equivalent width with respect to that continuum as it does when it is directly observed. This would result in a red wing similar to that observed. The fact that some of the line profiles extend to energies lower than could easily be produced by Compton scattering in a cold medium suggests that the red wings may indeed be associated with the relativistic disk component seen in scattered light. However, uncertainties in the continuum modelling used to produce the line profiles may make such a conclusion premature.

The presence of the high-ionization lines make the average line profile from group C significantly different to that obtained for a sample of Seyfert 1 galaxies (N97) (which shows a strong broad red-wing but no high-ionization species of iron Kα). While the two types of Seyfert galaxy may well contain iron Kα line components from all the same regions the high-ionization lines would be swamped by the direct continuum in the Seyfert 1 case.

If these high-ionization iron K-shell lines arise in the scattering gas, then in the model of Heisler, Lumsden and Bailey (1997), we might expect to preferentially detect these species in sources for which a hidden BLR has been detected in the scattered optical light. This is because their model places the scattering region within the obscuring torus, so hidden BLRs are visible when sources are observed from lines-of-sight which skim the edge of the torus, i.e. for a narrow range of observing angles. For sources viewed at a favorable angle the torus hides the central engine and BLR, but allows direct observation of the scattering gas. For sources viewed more edge-on, the scattering region is also hidden. Our data are consistent with that idea, in that we detect these line species in all the sources where we see

the BLR in scattered optical light and for which we have sufficient signal-to-noise ratio in the X-ray spectra to tell.

We would expect to observe emission lines other than iron-K from the scattering gas, particularly at soft X-ray energies, and indeed many such lines are observed (Paper I). Ideally, then, one would wish to compare detailed photoionization models for the scattering region with our data to determine the physical characteristics of the gas. However, some ambiguity remains as to whether the observed soft X–ray lines arise via nuclear processes, or are related to starburst activity. Furthermore, high-ionization iron–K species are detected in sources such as NGC 5135, which has a strong starburst component. This raises the question as to whether some of the iron Kα emission might arise from non-nuclear processes. Clearly, separating the emission of the Seyfert from that of the starburst is necessary for a conclusive answer.

5. Starburst contributions to the X-ray Flux

Starburst emission is a well-documented phenomenon in many Seyfert 2 galaxies. It is not yet clearly established as to whether starburst activity occurs at the same level in Seyfert 1 galaxies. Some studies indicate a similar star formation rate in Seyfert 1 galaxies and starburst galaxies (Yamada 1994) while others indicate that the host galaxies of type-2 nuclei have significantly higher levels of starburst activity than type-1 nuclei (Maiolino et al. 1995). If it does occur at the same level in the two types of Seyfert, the X-ray emission associated with the starburst would be swamped by the Seyfert 1 nuclei. For a sample of obscured AGN, we would expect some observable differences as the degree of nuclear obscuration varies between sources and hence the contrast is changed between contributions from the host galaxy versus the nucleus. In Paper I we found that in the 0.5-4.5 keV band the estimated average contribution from starbursts in the host galaxy was $\sim 60\%$ for the Seyfert 2 galaxies, versus 2% for the NELGs. We also noted that soft X-ray lines were observed in many Seyfert 2 galaxies, but in none of the NELGs (Paper I). As strong soft X-ray lines are seen in some starburst galaxies (Ptak et al. 1997), these facts necessitate careful consideration of the the starburst contribution to the X-ray flux.

Unfortunately, the *ASCA* data do not allow us to spatially deconvolve the X-ray lines produced by starburst activity from those produced in the scattering gas. However, Wilson et al. (1992) find that the starburst disk in NGC 1068 can provide a 2-10 keV flux of $\sim 2 - 8 \times 10^{-12}$erg cm^{-1}s^{-1}, consistent with all of the *ASCA* flux. So, although the high equivalent widths and energies of the iron Kα lines link them with reflection or scattering of nuclear radiation, some or all of the other X-ray emission lines may be attributable to

starburst activity.

Examining the level of starburst "contamination" for targets in group C, we find just one source which is not significantly contaminated by a starburst component, Mrk 3 (Paper I and Pogge & De Robertis 1993). This source is particularly interesting as, despite the lack of starburst emission, it does show significant soft X-ray emission lines. Mrk 3 is one of the brightest Seyfert 2 galaxies with a hidden BLR. Detailed analysis of the optical data has shown the broad lines have a polarization of 20% (Tran 1995b). Although there has been some debate over the Hubble type of the host galaxy for Mrk 3, it is now thought to reside in an elliptical host galaxy (Jenkins 1981, Wagner 1987), and it has a radio jet with knots and a large bright radio lobe (Kukula et al. 1993). This source offers us the best opportunity available to date to obtain information about conditions in the X-ray reprocessing regions of a Seyfert 2 galaxy.

6. A case study: Mrk 3

We constructed a spectral model table of the emission spectrum from a slab of photoionized gas illuminated by an ionizing continuum using the ION photoionization code. ION includes the important excitation and ionization processes, full temperature and radiative transfer solutions, while emission, absorption and reflection by the gas are calculated asuming thermal and ionization equilibrium. The model tables we use assume a photon index $\Gamma = 2.0$ in the 0.2 – 50 keV range, and $\Gamma = 1.5$ from 1.6 – 40.8 eV. The optical to X-ray energy index is assumed to be $\alpha = 1.5$. Cosmic abundances were used, and a constant density $n_H = 10^{10}\mathrm{cm}^{-3}$ throughout the slab. The X-ray ionization parameter is defined as

$$U_X = \int_{0.1\ \mathrm{keV}}^{10\ \mathrm{keV}} \frac{Q(E)}{4\pi r^2 n_H c} dE \qquad (1)$$

where $Q(E)$ is the number of photons at energy E, r the distance from the source to the illuminated gas. For more details of the ION code see Netzer (1993; 1996). The absorption of this component was fixed at the Galactic value $8.7 \times 10^{20}\mathrm{cm}^{-2}$. In addition to this component we allowed a pure Compton-reflection spectrum utilizing the model of Magdziarz & Zdziarski (1995) plus a gaussian line (since their reflection model does not include line emission). We assumed reflection of a $\Gamma = 2.0$ continuum (with no exponential cut-off; the data do not allow us to determine whether any cut-off is present) from relatively neutral material (only H and He are ionized) viewed face-on. This model provided a good fit to the data yielding $\chi^2 = 349/328$.

6.1. The Hard X-ray Spectrum

The energy at which the primary continuum becomes visible depends on the column obscuring it. If the nucleus of Mrk 3 was obscured by a column $\sim 10^{24}\mathrm{cm}^{-2}$ as observed in NGC 4945, then the direct continuum component should become observable close to $\sim$ 10 keV. In fact the *ASCA* spectrum does show a small hard tail compared to the Compton-reflection model noted above. The *ASCA* fit improves by $\Delta\chi^2 \sim$11 on addition of a highly absorbed power-law component of fixed index $\Gamma = 2$. This component is absorbed by a column of $N_H = 1.3^{+2.2}_{-0.6} \times 10^{24}\mathrm{cm}^{-2}$, and provides 25% of the 5-10 keV observed flux. We estimate the intrinsic (unabsorbed) 2-10 keV luminosity of this nuclear component to be $\sim 10^{43}\mathrm{erg\ s}^{-1}$. The reflecting medium is implied to subtend $\Omega \sim 2 \pm 1\pi$ steradians to the intrinsic continuum source. This model is shown in Fig. 6, along with the data/model ratio.

Iwasawa et al. (1994) find a different solution to the *ASCA* spectral data, with a model in which the direct absorbed continuum component dominates the 3 – 10 keV spectrum, absorbed by $N_H \sim 4 \times 10^{23}\mathrm{cm}^{-2}$. No reflection component is included in their model. However, the observed equivalent width in iron Kα is 977^{+193}_{-137} eV (when modelled as a narrow line, Paper I), which requires a column of $10^{24}\mathrm{cm}^{-2}$ in order for the line to be produced by transmission (Fig. 1), assuming a Leahy & Creighton (1993) geometry. The upper limit on column yielded by the Iwasawa et al. (1994) solution is $5.8 \times 10^{23}\mathrm{cm}^{-2}$, which is too low to produce the line, assuming the Leahy & Creighton geometry is applicable.

Our model, which includes the Compton-reflection component, yields a better fit by $\Delta\chi^2 = 59$ (obtained by comparing the fit of their model and ours using our datasets). The inclusion of a Compton-reflection component also provides a natural explanation for the very flat $\Gamma = 1.30 \pm 0.3$ spectrum observed in the *Ginga* data (Awaki et al. 1990). The inclusion of the reflection component is the reason we obtain a higher column for the direct component than Iwasawa et al. (1994), in fact our column of $\sim 10^{24}\mathrm{cm}^{-2}$ is consistent with the strength of the iron Kα line. That line is now consistent either with an origin in the line-of-sight material or via Compton reflection alone. The indication that the line flux variations are correlated with the hard X-ray continuum variations favors the latter (see §6.3).

6.2. The soft X-ray Spectrum

The soft part of the spectrum (below $\sim$ 3 keV) is well modelled by the emission from a photoionized plasma with $U_X = 4.8^{+1.5}_{-1.3}$ and $N_H = 3.5^{+1.7}_{-1.4} \times 10^{23}\mathrm{cm}^{-2}$. This highly ionized gas can produce the 6.96 keV component of the iron line and the Si and S lines and

scatters some of the nuclear radiation into our line-of-sight. This component is much more highly ionized than the zone of material comprising the warm absorber evident in *ASCA* observations of Seyfert 1 galaxies (when a single-zone model is assumed for the latter). The temperature of the gas is $\sim 10^5$ K, consistent with that of the optical scattering gas in NGC 1068 (Miller, Goodrich & Mathews 1991)

However, this soft X-ray flux might have some contribution from shocked gas. Recent *HST* observations (Capetti et al. 1995) have resolved a sub-arcsec region of continuum emission, which they propose could either be associated with gas which is shocked by passage of the jet, or the BLR scattering gas. Those authors also show a $\sim 2''$ S-shaped region of narrow line gas, although this gas is photoionized by the central AGN, it is too cool to produce the soft X-rays emission observed.

The absorption-corrected 2-10 keV luminosity in the ionized-gas component alone is 5×10^{41}erg s^{-1}. The scattered fraction of flux is proportional to the product of the scattering efficiency and the solid angle of the scattering material. Assuming the scattering gas dominates over shock-heated gas, then our X-ray data indicate a scattered X-ray fraction of $\sim 5 \pm 1\%$. This is comparable to the few percent generally derived from optical measurements of type-2 AGN (e.g. Pier et al. 1994). The estimate of intrinsic 2-10 keV luminosity from the [OIII] line flux is 2×10^{44}erg s^{-1}, yielding an estimate of 0.25% for the scattered fraction. Alternatively, using the Mulchaey (1994) relationship between infrared and hard X-ray luminosity we estimate an intrinsic luminosity of 6.6×10^{43}erg s^{-1} and a scattered fraction 0.75%.

6.3. Constraints from variability

If the hard X-ray emission is transmitted through the obscuring material in our line-of-sight, then we will observe the hard X-ray variations of the nucleus directly. Alternatively, if the hard X-ray emission is dominated by a reflected component, then the light curve of the reprocessed emission will lag the primary emission and be smoothed. The degree of lag and the smoothing depend on the location and size of the reprocessor and its geometry.

The soft X-ray flux has not varied over the ~ 13 year baseline for which we have flux measurements (Iwasawa et al. 1994), suggesting that it comes from an extended region. If this flux is associated with the $0.35 \times 1''$ bar of continuum emission resolved by *HST* (Capetti et al. 1995), then it originates in a region several hundred pc in size.

However, the hard X-ray emission of Mrk 3 is variable. The fastest historical change

in the hard flux was a factor of 2 drop between the *Ginga* and *BBXRT* observations, taken one year apart. The 6.4 keV line flux appears to vary in a way which is consistent with that change in the continuum while the soft X-ray flux remains steady, ruling out a lag between the reprocessed and nuclear flux as the explanation for the high equivalent width.

The observed variability places a rough constraint on the size of the variable source to be < 0.3 pc. The shape of the spectrum suggests that the nucleus is not observed directly and therefore this constraint applies to the reprocessing material, rather than the central source. This could have a small scale-height, in fact Gallimore et al. (1996) suggest that a pc-scale maser disk with toroidal geometry exists in NGC 1068, based on a water maser observation. This disk is observed at high inclination (82^o) and can provide sufficient opacity to block the X-ray continuum below 10 keV.

7. Discussion and Conclusions

Consideration of the iron Kα, [OIII] line and X-ray variability indicates that the *ASCA* observations are dominated by reprocessed X-rays in the cases of NGC 1068, NGC 4945, NGC 2992, Mrk 3, Mrk 463E and Mrk 273.

The iron Kα line profiles of these sources show significant contributions from neutral and high-ionization species of iron. Thus it appears that Compton reflection, the hot scattering gas and/or starburst emission contribute to the 5-7 keV regime.

Mrk 3 shows negligible starburst contamination, so the X-ray spectrum is probably dominated by processes intimately related to the active nucleus. The *ASCA* spectrum can be described by hot scattering gas in the soft X-ray regime, with $U_X \sim 5$, $N_H \sim 4 \times 10^{23}\mathrm{cm}^{-2}$. This material is more highly ionized than the zone of material comprising the warm absorber seen in Seyfert 1 galaxies, but may have some contribution from shock-heated gas associated with the jet. Estimates of the scattering fraction cover 0.25 – 5%. The hard X-ray spectrum of this source appears to be dominated by a Compton-reflection component although there is evidence that the primary continuum component becomes visible close to ~ 10 keV.

It is obvious that a big problem with analysis of X-ray observations of type-2 Seyferts to date has been the inability to deconvolve the starburst emission (and any other extended thermal gas) from that in the immediate environment of the nucleus (and while *ROSAT* provided several arcsecond spatial resolution it offered data over a narrow bandpass with low spectral resolution). *HST* observations have now resolved a 1-2 arcsec region in which the UV scattering occurs in NGC 1068 (Antonucci et al. 1994), corresponding to a region

$\sim 110-220$ pc in size. The *AXAF* High Resolution Camera (HRC) will allow sub-arcsecond X-ray imaging. Assuming the UV scattering region is closely related to the X-ray scattering region, then we will be able to spatially resolve the X-ray "mirror" for the first time in NGC 1068, other nearby sources such as NGC 4945 and NGC 1808 and we will be able to resolve the bar of emission observed in Mrk 3 by *HST*. If the X-ray scattering gas turns out to be the same gas which is observed as a warm absorber in Seyfert 1 galaxies, then such imaging may map the distribution of the warm absorber. As the starburst emission often extends over regions many tens of arcseconds or larger for nearby AGN, AXAF spectra should allow us to separate the starburst and nuclear components for at least some AGN. *Beppo SAX* and *XTE* also offer an opportunity to acquire X-ray spectra above 10 keV, which might help us determine the true nature of Mrk 3.

8. Acknowledgements

We are grateful to *ASCA* team for their operation of the satellite, to Keith Gendreau for discussions on *ASCA* calibration issues, Hagai Netzer for use of model tables generated using the photoionization code ION and Andy Ptak for comments on the properties of starburst galaxies. This research has made use of the Simbad database, operated at CDS, Strasbourg, France; of the NASA/IPAC Extragalactic database, which is operated by the Jet Propulsion Laboratory, Caltech, under contract with NASA; and data obtained through the HEASARC on-line service, provided by NASA/GSFC. We acknowledge the financial support of Universities Space Research Association (IMG, TJT) and the National Research Council (KN).

REFERENCES

Antonucci, R., 1993, ARA&A, 31, 473

Awaki, H., Koyama, K., Kunieda, H., Tawara, Y., 1990, Nature, 346, 544

Capetti, A., Macchetto, F., Axon, D.J., Sparks, W.B., Boksenberg, A., 1995, ApJ 448, 600

Dickey, J.M., Lockman, F.J., 1990, ARA&A, 28, 215

Done, C., Madejski, G.M., Smith, D., 1996, ApJ, 463, L63

Elvis, M., Lawrence, A., 1988, ApJ 331, 151

Elvis, M., Lockman, F.J., Wilkes, B., 1989, AJ, 97, 777

Gallimore, J.F., Baum, S.A., O'Dea, C.P., Brinks, E., Pedlar, A., 1996, ApJ 462, 740

George, I.M., Turner, T.J., Netzer, H., Nandra, K., Mushotzky, R.F., Yaqoob, T., 1997, ApJS submitted

George, I.M., Fabian, A.C. 1991, MNRAS 249, 352

Ghisellini, G., George, I.M., Fabian, A.C., Done, C., 1991, MNRAS 248, 14

Ferrarese, L., Ford, H.C., Jaffe, W., 1996, 470, 444

Fukazawa, Y., et al. 1994, PASJ 46, 141

Iwasawa, K., Yaqoob, T., Awaki, H., Ogasaka, Y., 1994, PASJ 46, L167

Haniff, C.A., Wilson, A.S., Ward, M.J., 1988, ApJ, 334, 104

Heisler, C.A., Lumsden, S.L., Bailey, J.A., 1997, Nature, 385, 700

Inglis, M.D. et al. 1997, MNRAS 263, 895

Iwasawa, K., Fabian, A.C. & Matt, G., 1996, MNRAS in press

Jenkins, C.R., 1981, MNRAS 197, 829

Krolik, J.H., Kriss, G.A., 1995, ApJ 447, 512

Kukula, M.J., Ghosh, T., Pedlar, A., Schilizzi, R.T., Miley, G.K., de Bruyn, A.G., & Saikia, D.J., 1993, MNRAS, 264, 893

Lawrence, A., 1991, MNRAS, 252, 586

Leahy, D.A. & Creighton, J. 1993, MNRAS 263, 314

Marshall, F. et al. 1993, ApJ 405, 168

Maiolino, R., Rieke, G.H., 1995, ApJ 454, 95

Matt, G., Perola, G.C., Piro, L., 1991, A&A, 247, 25

Matt, G., Brandt, W.N., Fabian, A.C., 1996, MNRAS 280, 823

Miller, J.S., Goodrich, R., 1990, ApJ 355, 456

Miller, J.S., Goodrich, R., Mathews, W.G., 1991, ApJ 378, 47

Mulchaey, J.S., Koratkar, A., Ward, M.J., Wilson, A.S., Whittle, M., Antonucci, R.J., Kinney, A., Hurt, T., 1994, ApJ 436, 586

Nandra, K., George, I.M., Mushotzky, R.F., Turner, T.J., Yaqoob, T., 1997, ApJ, in press

Netzer, H., 1993, ApJ 411, 594

Netzer, H., 1996, ApJ 473, 781

Pier, E.A., Antonucci, R., Hurt, T., Kriss, G., Krolik, J., 1994, ApJ 428, 124

Pogge, R.W., 1988, ApJ, 328, 519

Ptak, A., Serlemitsos, P, Yaqoob, T., Mushotzky, R.F., Tsuru, T. 1997, AJ, sched for April issue

Pogge, R.W., De Robertis, M.M., 1993, ApJ, 404, 563

Polletta, M., Bassani, L., Malaguti, G., Palumbo, G.G.C., Caroli, E., 1996, ApJS 106, 399

Tadhunter, C., Tsvetanov, Z., 1989, Nature, 341, 422

Tran, H., 1995a, ApJ 440, 597

Tran, H., 1995b, ApJ 440, 574

Turner, T.J., George, I.M., Nandra, K., Mushotzky, R.F., 1997, ApJS, submitted

Turner, T.J., George, I.M., Nandra, K., Mushotzky, R.F., 1997b, ApJ, submitted

Ueno, S. et al. 1997, In "X-ray Imaging & Spectroscopy of Cosmic Hot Plasmas", March 11-14 1996, Tokyo.

Wagner, S.J., 1987, A&A, 185, 77

Weaver, K.A., Nousek, J., Yaqoob, T., Mushotzky, R.F., Makino, F., Otani, C., 1996a, ApJ 458, 160

Wilson, A.S., Elvis, M., Lawrence, A., Bland-Hawthorn, A., 1992, ApJ 391, L75

Yamada, T., 1994, ApJ 423, L27

Figure Captions

Fig 1 - Equivalent width of the narrow 6.4 keV line versus absorbing column (from Paper I). The dot-dash line shows the line equivalent width expected from a uniform shell of material encompassing the continuum source (Leahy & Creighton 1993). The dashed line shows the predicted equivalent width from reflection as a function of $N_{\rm H}$, assuming that only the power-law is absorbed, but that the reflection component remains unchanged. Data points are annotated with an abbreviation of the source name. Group A sources are marked as circles, group B sources as stars and group C sources as squares (see §3.3). A few of the lowest signal-to-noise datasets have not been classified.

Fig 2 - The predicted intrinsic 2-10 keV luminosity, based upon the [OIII] line flux (see text for details) versus the observed (absorption-corrected) luminosity. We have annotated those sources having predicted luminosities more than a factor of 15 greater than the observed values. Again, group A sources are marked as circles, group B sources as stars and group C sources as squares (§3.3).

Fig 3 - The emission spectrum from a warm absorber including scattered continuum emission (from a $\Gamma = 2$ power-law) plus thermal and line emission from the hot gas. The gas has an ionization parameter $U_X \sim 0.12$ and column $N_H \sim 4 \times 10^{22}{\rm cm}^{-2}$, based on the analysis of *ASCA* observations of Seyfert 1 galaxies (see George et al. 1997).

Fig 4 - The data/model ratios versus the best-fit simple continuum model for NGC 1068, Mrk 3, NGC 2992, and NGC 4945 (from Paper I). The X-axis shows the observed-frame energy. In the left hand panels data from all four instruments have been combined for clarity. In the right hand panels, the two SIS datasets have been combined. The data are in 50 eV bins up to 3 keV, 100 eV bins between 3 and 7 keV and 200 eV bins in the 7-10 keV range. An excess of counts is generally evident in the 5-7 keV data, versus the continuum model. This indicates the presence of strong iron K-shell emission lines in most objects.

Fig 5 - The average data/model ratio in the iron Kα regime. The group C datasets were used to create the mean ratio. Each dataset was corrected to the rest-frame energy before the objects were combined and so the X-axis shows the rest-frame energy. The dotted Gaussian profile represents the SIS instrument response for a narrow line observed at a rest-energy of 6.4 keV.

Fig 6 - The best fit model to the *ASCA* spectral data for Mrk 3, along with the data/model ratio. The SIS and GIS ratios have been combined for clarity of illustration. The model comprises an emission spectrum from highly ionized gas, a Compton-reflection component and an absorbed power-law (see §6). A Galactic column of $8.7 \times 10^{20}{\rm cm}^{-2}$

covers all components.

Table 1. The *ASCA* Seyfert 2 sample.

Name	RA[a]	DEC[a]	z[a]	Class[a]	L_X	$L_{[OIII]}$
MCG-01-01-043	00 10 03.5	-04 42 18	0.0300	S2	42.88	···
NGC 526A	01 23 55.1	-35 04 04	0.0192	NELG[b]	43.77	43.49
NGC 1068	02 42 40.8	-00 00 47	0.0038	S2[b]	41.15	43.95
NGC 1667	04 48 37.2	-06 19 12	0.0152	S2	40.46	42.69
E0449-184	04 51 38.8	-18 18 55	0.338	S2	44.86	···
NGC 1808	05 07 42.3	-37 30 46	0.0033	SB/S2	40.62	40.69
NGC 2110	05 52 11.4	-07 27 22	0.0076	NELG	42.82	42.49
Mrk 3	06 15 36.3	71 02 15	0.0135	S2[b]	42.33	44.30
NGC 2992	09 45 41.9	-14 19 35	0.0077	NELG[b]	42.05	43.23
MCG-5-23-16	09 47 40.2	-30 56 54	0.0083	NELG[b]	43.43	42.69
NGC 4507	12 35 36.5	-39 54 31	0.0118	S2	42.28	43.68
NGC 4945	13 05 26.2	-49 28 16	0.0019	S2	40.53	···
NGC 4968	13 07 06	-23 40 43	0.0100	S2	42.45	42.50
NGC 5135	13 25 44	-29 50 01	0.0137	S2	43.16	43.11
NGC 5252	13 38 15.9	04 32 33	0.0230	S1.9	43.24	43.56
Mrk 273	13 44 42.1	55 53 13	0.0378	S2	42.45	44.03
Mrk 463E	13 56 02.9	18 22 19	0.0500	S2[b]	42.75	44.75
NGC 5695	14 37 22.0	36 34 04	0.0141	S2	< 40	42.65
NGC 6251	16 32 31.9	82 32 17	0.0230	S2	42.50	41.94
NGC 6240-49	16 52 59.3	02 23 59	0.0245	S2	43.61	42.69
ESO 103-G35	18 38 20.2	-65 25 42	0.0133	S2/NELG	43.14	42.84
IC 5063	20 52 02.9	-57 04 14	0.0113	S2[c]	43.15	43.57
NGC 7172	22 02 02.1	-31 52 12	0.0086	S2/NELG[b]	43.22	···
NGC 7314	22 35 45.7	-26 03 03	0.0047	S1.9/NELG	42.59	41.63
NGC 7582	23 18 23.2	-42 22 11	0.0053	S2/NELG[d]	42.32	42.65

[a]From the NASA Extragalactic Database (NED);
[b] [c] [d] Polarized broad lines have been detected: (b) Tran 1995, (c) Inglis et al. 1993, (d) Heisler, Lumstron, Bailey 1997

Note. — Group C sources are bold-face. Column 1: Name; Columns 2 & 3: RA & DEC, J2000; Column 4: Redshift; Column 5: Seyfert type, SB= starburst galaxy, NELG=Narrow-Emission-Line Galaxy; Column 6: Observed 2-10 keV luminosity (absorption corrected, but see §4.1); Column 7: Intrinsic 2-10 keV luminosity inferred from [OIII] fluxes

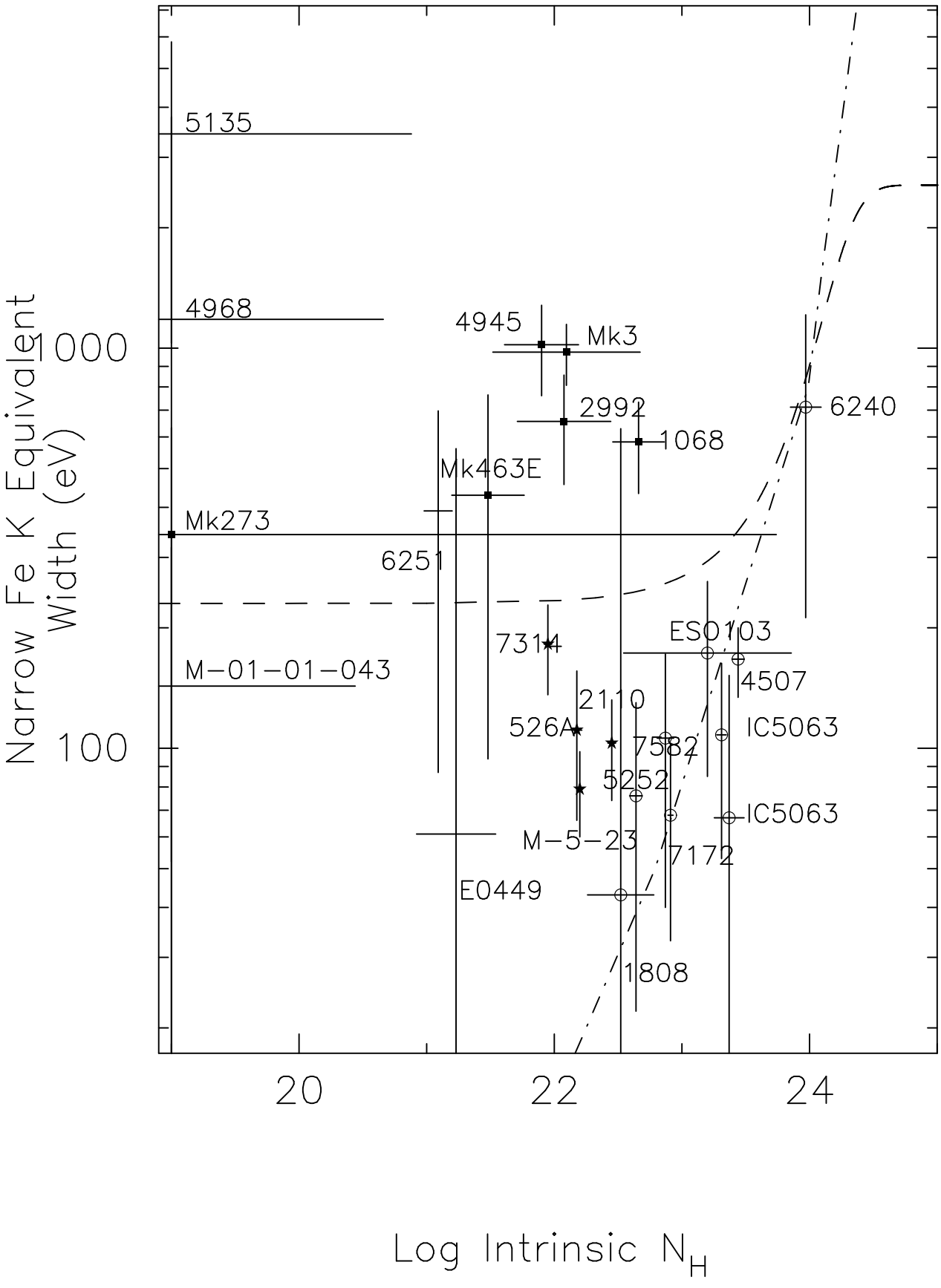
Narrow Fe K Equivalent Width (eV)
1000
100
20
22
24
Log Intrinsic N_H
5135
4968
Mk273
M−01−01−043
4945
Mk3
2992
1068
Mk463E
6251
6240
7314
ESO103
4507
2110
526A
IC5063
7582
5252
IC5063
M−5−23
7172
E0449
1808

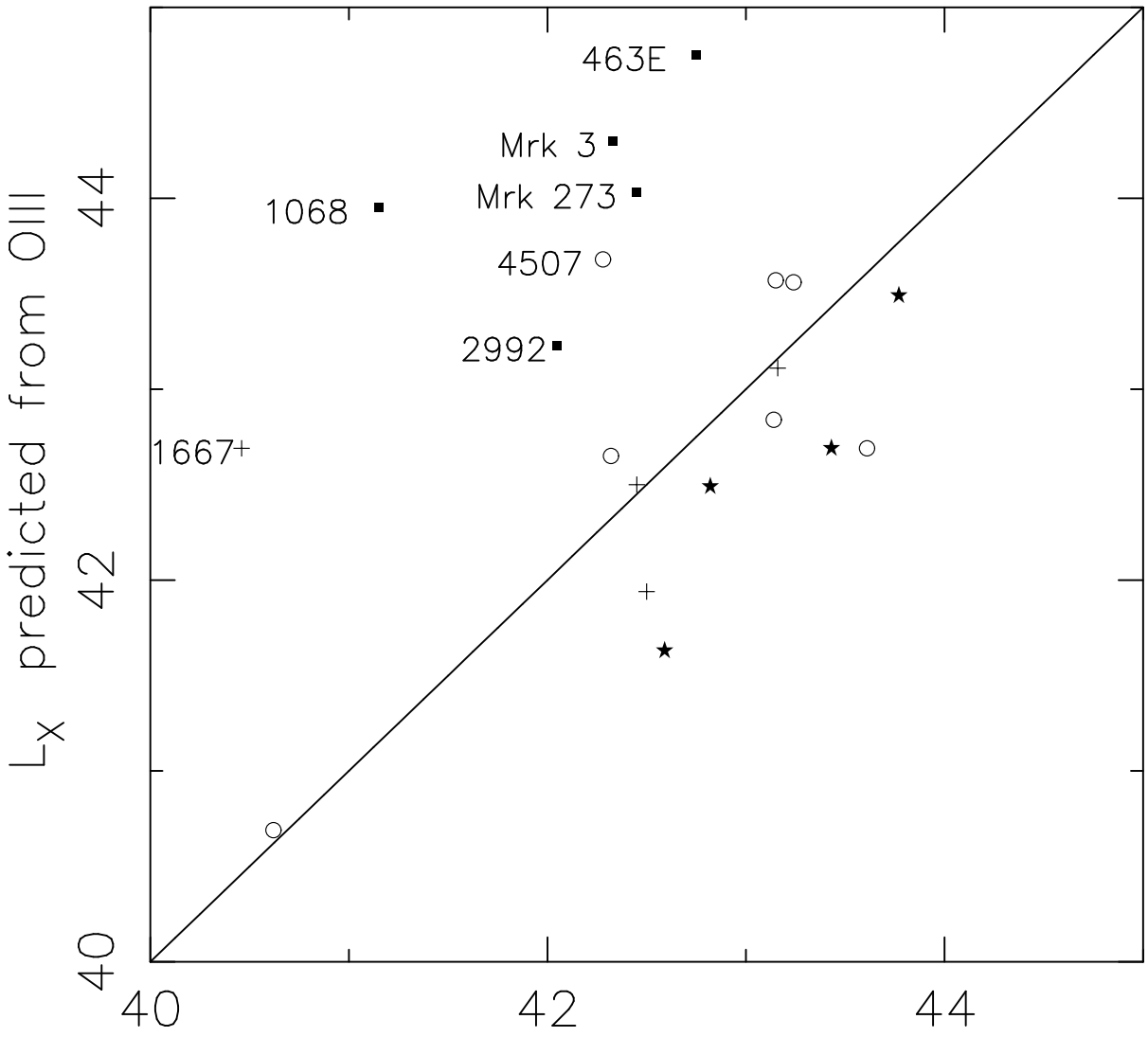
463E
Mrk 3
Mrk 273
1068
4507
2992
1667+
L_X predicted from OIII
40
42
44
40
42
44

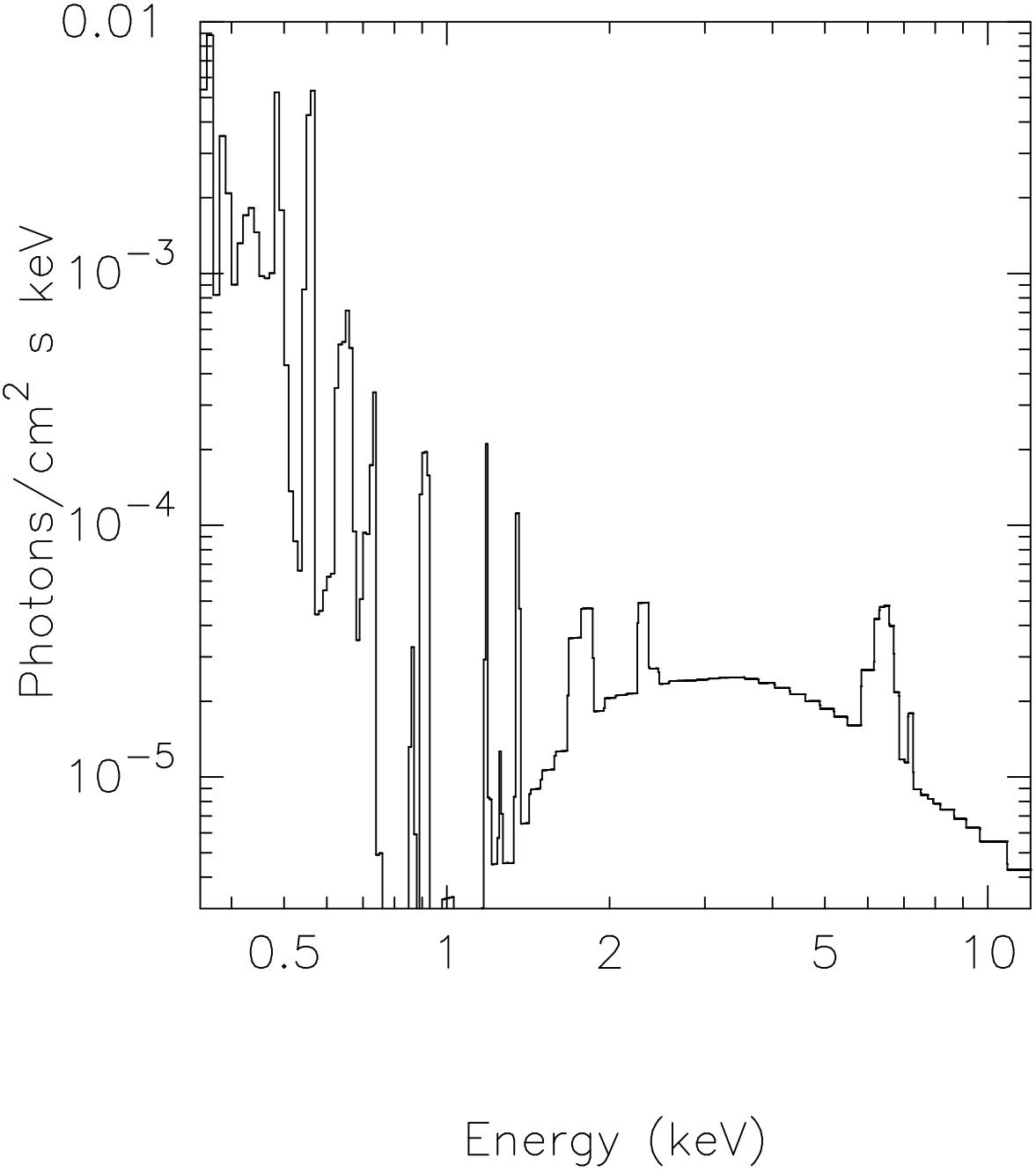
0.01
10^{-3}
10^{-4}
10^{-5}
Photons/cm^2 s keV
0.5
1
2
5
10
Energy (keV)

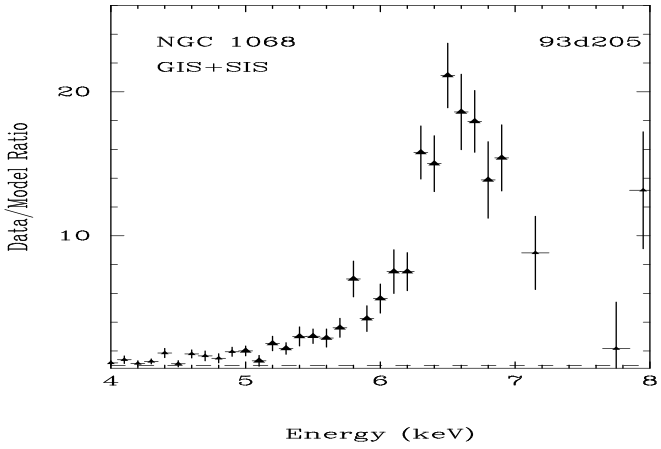
NGC 1068
GIS+SIS
93d205
Data/Model Ratio
Energy (keV)

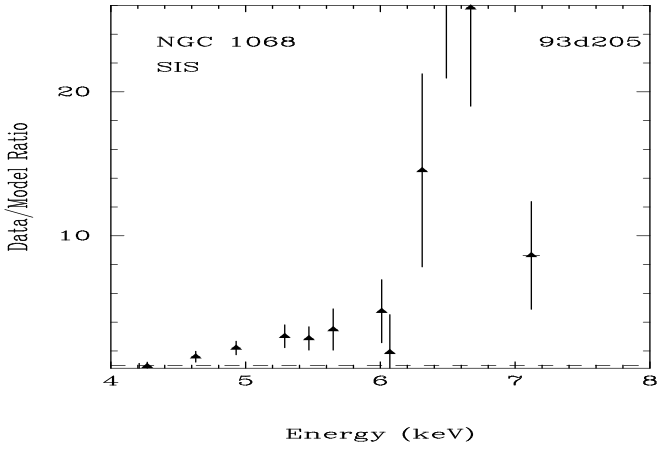
NGC 1068
SIS
93d205
Data/Model Ratio
Energy (keV)

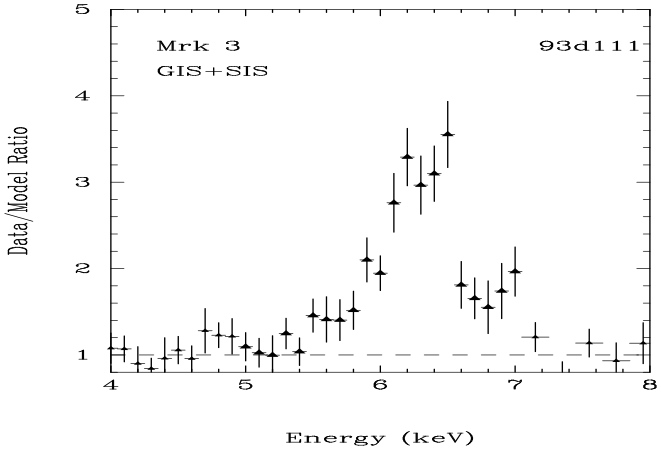
Mrk 3
GIS+SIS
93d111
Data/Model Ratio
Energy (keV)

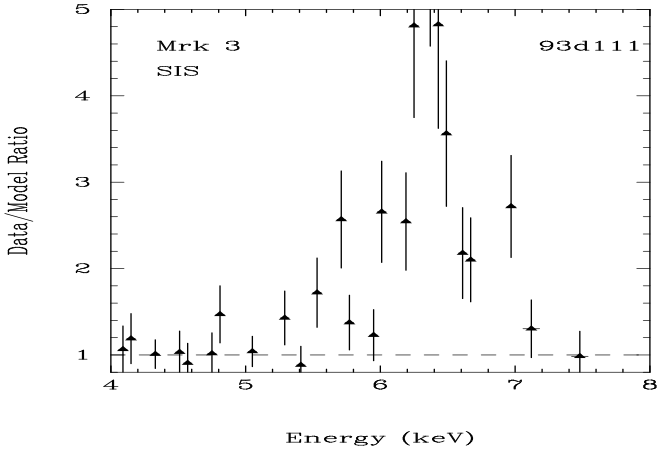
Mrk 3
SIS
93d111
Data/Model Ratio
Energy (keV)

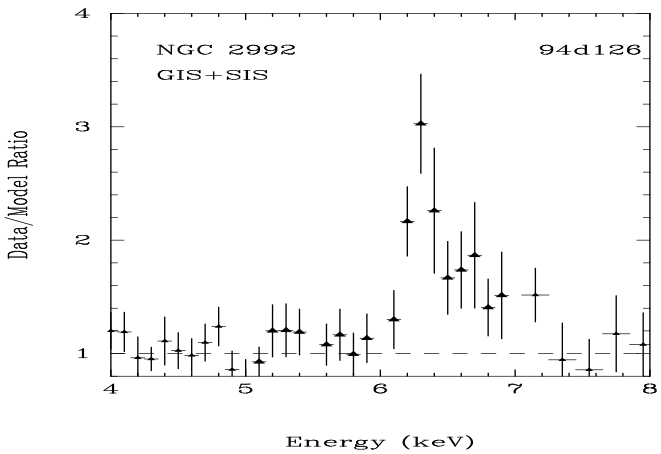
NGC 2992
GIS+SIS
94d126
Data/Model Ratio
Energy (keV)

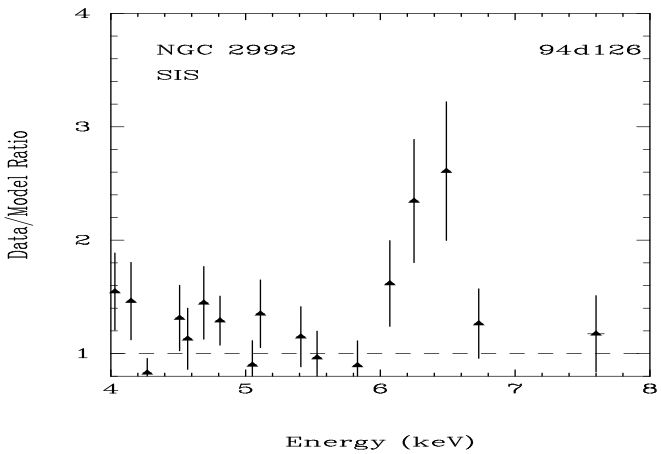
NGC 2992
SIS
94d126
Data/Model Ratio
Energy (keV)

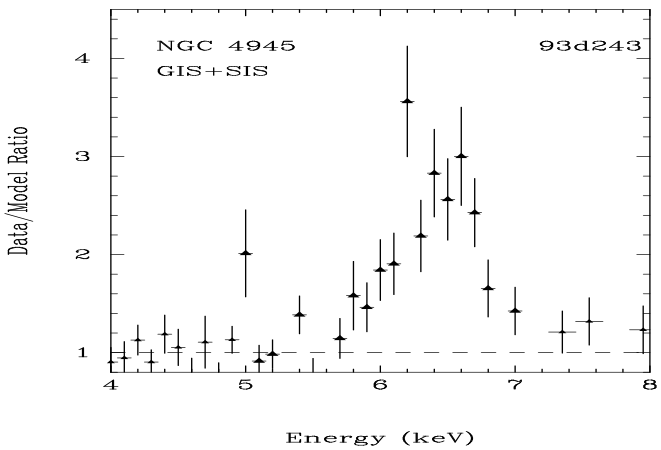
NGC 4945
GIS+SIS
93d243
Data/Model Ratio
Energy (keV)

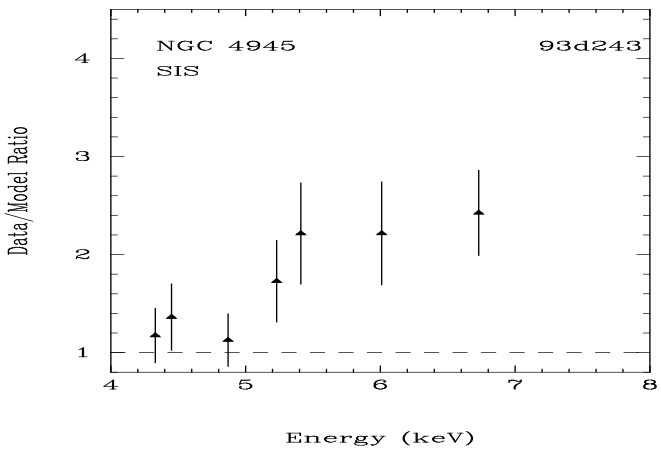
NGC 4945
SIS
93d243
Data/Model Ratio
Energy (keV)

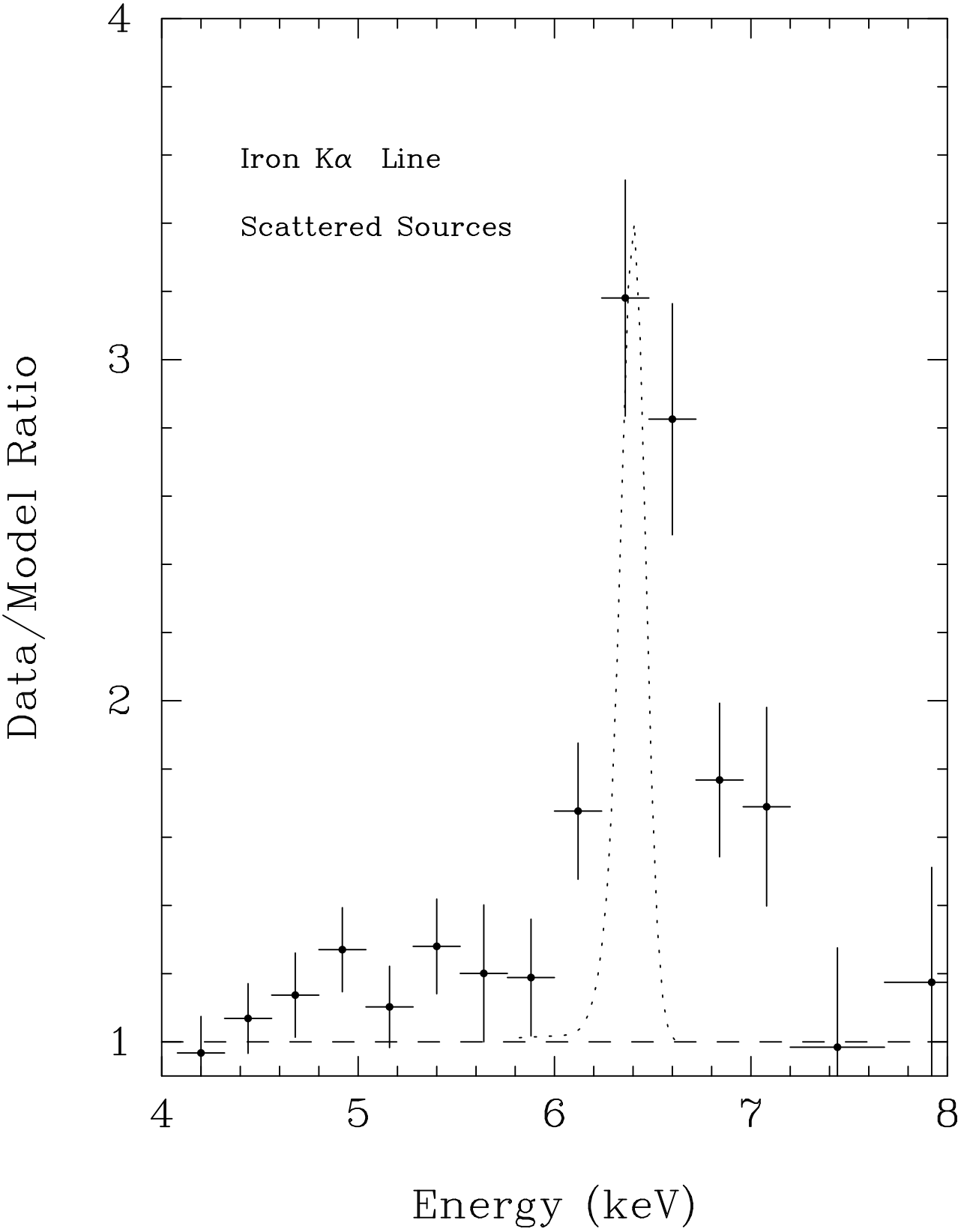
Iron Kα Line
Scattered Sources
Data/Model Ratio
Energy (keV)
1
2
3
4
4
5
6
7
8

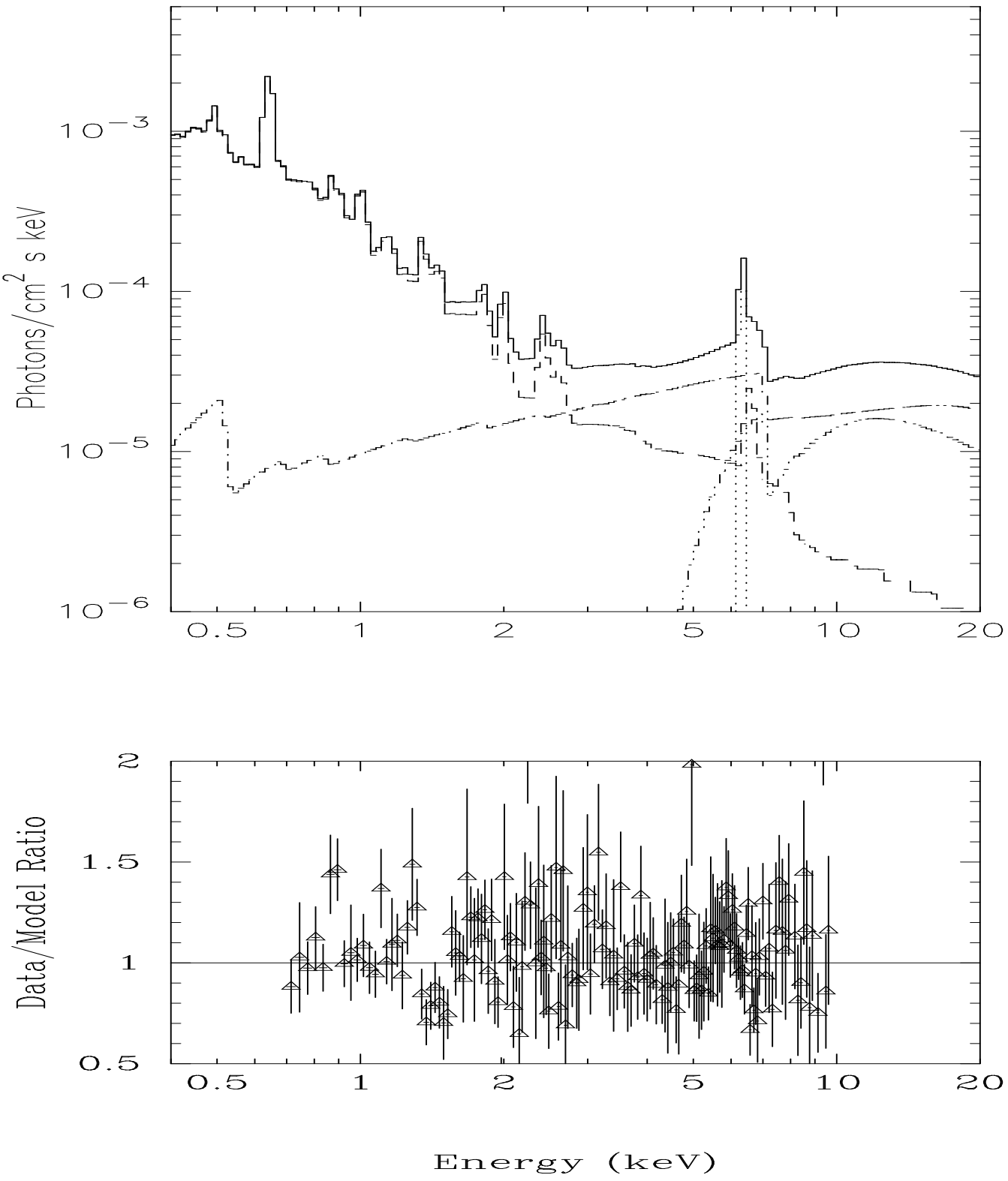
Photons/cm^2 s keV
10^{-3}
10^{-4}
10^{-5}
10^{-6}
0.5
1
2
5
10
20
Data/Model Ratio
2
1.5
1
0.5
0.5
1
2
5
10
20
Energy (keV)